Three-wave interactions between fast-ion driven modes in the National Spherical Torus Experiment

N. A. Crocker,[1] E. D. Fredrickson,[2] S. Kubota,[1] W. A. Peebles,[1] R. E. Bell,[2] S. M. Kaye,[2] B. P. LeBlanc,[2] and J. E. Menard[2]
[1]*Department of Physics and Astronomy, University of California, Los Angeles, California 90095, USA*
[2]*Princeton Plasma Physics Laboratory, Princeton, New Jersey 08543, USA*

(Received 11 February 2009; accepted 3 April 2009; published online 29 April 2009)

Experiments in the National Spherical Torus Experiment [M. Ono *et al.*, Nucl. Fusion **40**, 557 (2000)] have yielded new, unique observations of nonlinear three-wave interactions between compressional Alfvén eigenmodes (CAEs) and other fast-ion driven instabilities. Specifically, nonlinear interactions of CAEs have been conclusively identified with both energetic particle modes (EPMs) and toroidicity-induced Alfvén eigenmodes (TAEs). These nonlinear interactions occur simultaneously with other three-wave interactions observed between the TAEs and EPMs [N. A. Crocker *et al.*, Phys. Rev. Lett. **97**, 045002 (2006)]. The interaction between the CAEs and EPMs spatially redistributes the energy of the CAEs, concentrating it into a toroidally localized wave packet in the same way that the interaction between the TAEs and EPMs spatially concentrates the energy of the TAEs. The interaction between the CAEs and TAEs has been shown to further subdivide the CAE wave packet into a train of smaller wave packets. These nonlinear interactions occur during fast-ion loss events. The spatial redistribution of CAE fluctuation energy will modify the effect of the CAEs on fast-ion transport during these events. © *2009 American Institute of Physics*. [DOI: 10.1063/1.3124143]

I. INTRODUCTION

Fast-ion modes—plasma instabilities driven by energetic ions produced by neutral beam or ion cyclotron range of frequencies heating or by fusion alphas—can significantly impact the transport and confinement of fast ions, thereby impacting fusion performance. As consideration of the physics basis for ITER evolves, nonlinear processes are emerging as a significant factor in the dynamics of fast-ion modes and are therefore receiving increasing attention.[1] Recent experiments in the National Spherical Torus Experiment (NSTX) (Ref. 2) have yielded new, unique observations of the dynamics of fast-ion modes in a strongly nonlinear regime. Nonlinear *three-wave interactions*,[3] in particular, are observed to occur quite commonly between many different types of fast-ion modes over a wide range of plasma conditions. Recent results published in Ref. 4 demonstrate an example of such nonlinear interaction between two different types of modes identified[5–7] as energetic particle modes (EPMs)[8–11] and toroidicity-induced Alfvén eigenmodes (TAEs).[12,13] The results presented here extend the analysis in Ref. 4, revealing that in addition to the interaction between the EPMs and TAEs, other three-wave interactions occur simultaneously. Higher frequency modes identified[14,5,7] as compressional Alfvén eigenmodes (CAEs)[15–17] are shown to interact with both the EPMs and TAEs. All of these nonlinear interactions are observed to occur during fast-ion loss events, indicating that they play a role in fast-ion loss. Analysis shows that these nonlinear interactions lead to a spatial redistribution of both CAE and TAE fluctuation energies that will modify their effect on fast-ion orbits. The interaction between the CAEs and EPMs spatially concentrates the energy of the CAEs into a toroidally localized wave packet whose envelope is "phase locked" to the EPM. (That is to say, the envelope toroidally propagates locked to a particular phase of the EPM.) This is very similar to the way in which the interaction between the TAEs and EPMs spatially concentrates the energy of the TAEs.[4] The interaction between the CAEs and TAEs is shown to similarly subdivide the CAE wave packet into a train of smaller wave packets whose envelopes are phase locked to the carrier wave of the TAE wave packet.

This report is divided into six sections, including the Introduction. The conditions for the experiment are described in Sec. II. The experimental results are described in Sec. III. Analysis and discussion of the results are presented in Secs. IV and V. The report finishes with a summary in Sec. VI and acknowledgments.

II. EXPERIMENTAL CONDITIONS

These observations are made in the same diverted *L*-mode NSTX helium plasmas described in Ref. 4. For the typical plasma (shot 113546), the major and minor radii are $R=0.85$ m and $a=0.64$ m, respectively. The plasma has a Shafranov shift of 15 cm, placing the magnetic axis at $R=1.0$ m. The typical plasma has a peak current of $I_P=0.80$ MA, a vacuum toroidal magnetic field at the geometric axis (i.e., $R=0.85$ m) of $B_{T0}=0.44$ T, and is heated by two tangential 1 MW, 65 keV deuterium neutral beams. The plasma current ramps up to a flattop in the first 250 ms of the discharge and then ramps back to zero between $t\approx 450$ and 600 ms [Fig. 1(a)]. The deuterium neutral beams (with tangency major radii of 0.59 and 0.49 m, respectively) are injected into the plasma from $t\approx 60-400$ ms, for a total power of $P_{NB}=2$ MW [Fig. 1(a)]. Also, a high harmonic fast wave

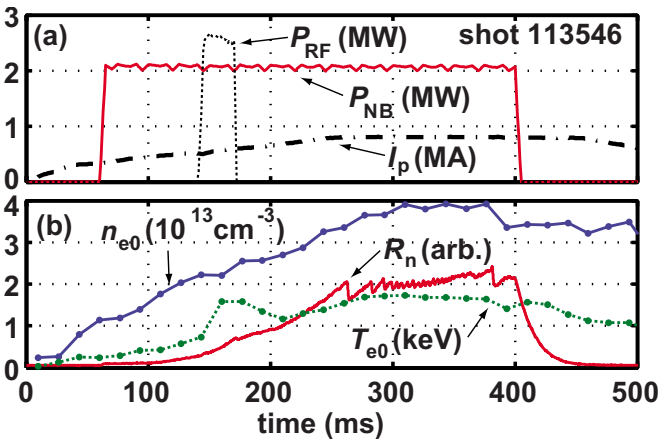

FIG. 1. (Color online) Time histories of (a) toroidal plasma current I_P, power from neutral beams P_{NB}, and high harmonic fast wave P_{RF}. (b) Central electron temperature and density, n_{e0}, and T_{e0}, and D–D fusion neutron production rate R_n (Ref. 4).

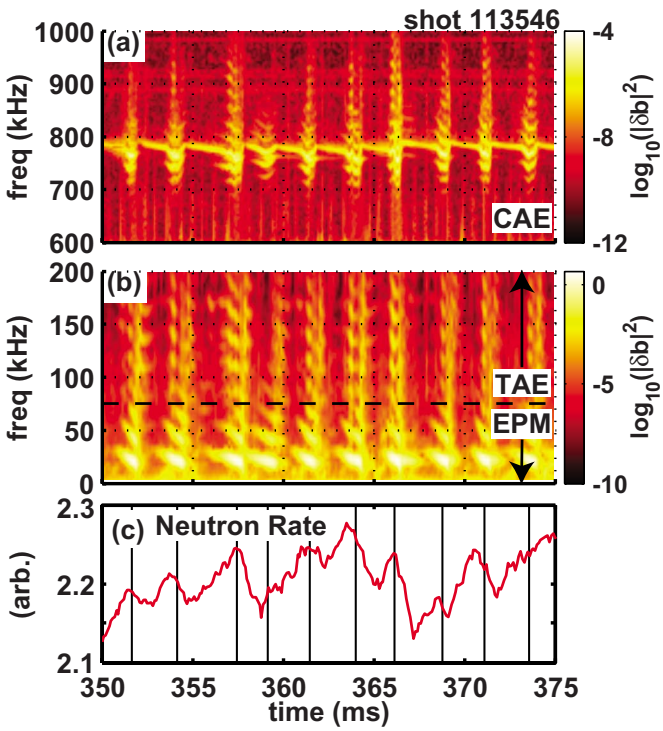

FIG. 2. (Color online) Edge magnetic spectrum of (a) CAEs and (b) EPMs and TAEs. Also, (c) D–D neutron rate with vertical lines showing time of maximum $n=1$ amplitude in each burst of magnetic fluctuations.

radio frequency ($f=30$ MHz) (Ref. 18) heating power of $P_{RF}=2.5$ MW is applied from $t\approx 140$ to 170 ms [Fig. 1(a)]. Multipoint Thomson scattering[19] shows that the central electron temperature and density (T_{e0} and n_{e0}), respectively, rise to peak values of ~ 1.7 keV and $\sim 3.85\times 10^{19}$ m^{-3} at ~ 300 ms and then gradually decrease [Fig. 1(b)]. This peak density results in a central Alfvén velocity of $v_{A0}\sim 1.1\times 10^6$ m/s, so the beam ions are ~ 2.3 times Alfvénic in the plasma center. The beams create a fast deuterium ion population in the plasma, which is signaled by a significant increase in the D–D fusion neutron rate R_n [Fig. 1(b)] over time. There are many drops in the neutron flux during the time period $t\sim 250-400$ ms which, as discussed below, correlate with bursts of mode activity. These drops indicate fast-ion loss.[20,21,5–7] The equilibrium modeling code EFIT,[22,23] constrained by external magnetic signals, indicates an elongation at the plasma boundary of $\kappa\sim 1.95$, a triangularity of $\delta\sim 0.45$, and safety factors of $q(r)\sim 1$ for $r\lesssim 30$ cm and $q_{95}\sim 7$ at the 95% flux surface. EFIT analysis also indicates $\beta_N\sim 3.76$, $\beta_P\sim 0.74$, and $\beta_T\sim 10\%$. Modeling by the equilibrium transport code TRANSP[24,25] estimates a central fast ion beta during the period of interest $t=350-375$ ms of $\sim 13\%$. This takes into account the neutral beam sources, the EFIT equilibrium, and assumes neoclassical transport for the fast ions. Charge exchange recombination spectroscopy[26,27] shows a plasma toroidal rotation frequency f_{rot} also during the period of interest, which is $\sim 30\times 10^3$ rotations/s for $r\lesssim 20$ cm, falling off in a roughly linear fashion to zero at the plasma edge.

III. EXPERIMENTAL RESULTS

In the plasmas described above, bursts of fluctuations occurring at ~ 2 ms intervals are observed which exhibit a rich spectrum of coherent modes. (Although transient in nature, the bursts last ~ 1 ms, which is sufficiently long that the modes—narrow-band, large amplitude spectral peaks—can be easily resolved.) These modes are detected by a range of diagnostics, including reflectometers probing the core plasma and Mirnov coils near the plasma edge. Figure 2 shows the time-dependent spectrum of magnetic fluctuations measured by one such Mirnov coil during the time period $t=0.350-0.375$ s, which includes several of the bursts. To obtain this time-dependent spectrum, the numerically integrated voltage measured by the coil is divided into records 0.25 ms long, overlapping by 0.125 ms, and a spectrum is calculated for each record. The records are conditioned with a Hanning window. As illustrated in Fig. 2(a), the bursts exhibit modes with frequencies in the range of $f\sim 600-1000$ kHz. They also exhibit modes grouped in the frequency range $f\sim 0-200$ kHz, as can be seen in Fig. 2(b) (Ref. 4). Figure 2(c) (Ref. 4) shows that these bursts coincide with $\sim 5\%$ drops in the D–D neutron rate, indicating that the observed modes play a role in fast-ion loss.[20,21,5–7]

The fast-ion modes illustrated in Figs. 2(a) and 2(b) can be divided into three groups. As discussed in Ref. 4, two of these groups, shown in Fig. 2(b), are identified as EPMs and TAEs. The EPMs have frequencies in the range $f\sim 0-75$ kHz and the TAEs have frequencies in the range $f\sim 75-200$ kHz. Measurements with the Mirnov coils near the plasma edge, which form a toroidally distributed array, were used to determine that the EPMs have toroidal mode numbers of $n\sim 1-2$ and that the TAEs have toroidal mode numbers of $n\sim 3-7$. (The sign convention used for n is that modes with positive n propagate in the same direction toroidally as the neutral beam ions and the plasma current.) Both the EPMs and TAEs are identified as fast-ion modes by their bursting character and the correlation of the bursts with sudden drops in the D–D neutron rate. The EPMs are identified as such by their characteristic low toroidal mode numbers and frequencies, in addition to the rapid, large downward

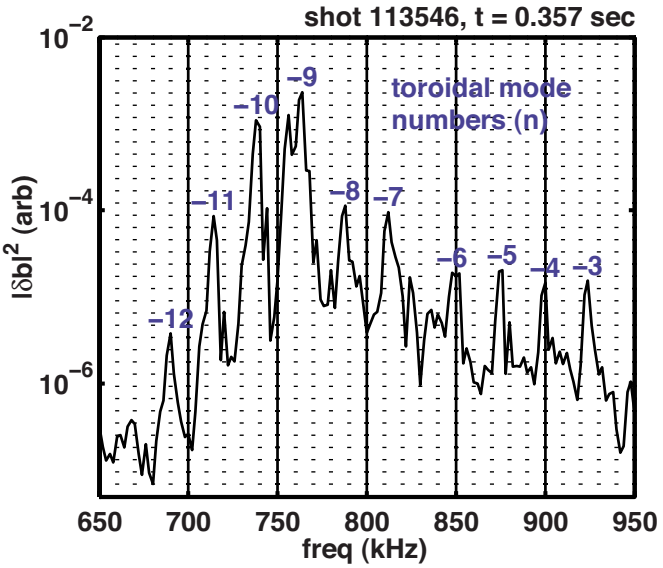

FIG. 3. (Color online) Magnetic spectrum at $t=0.357$ s showing CAEs with toroidal mode numbers (n) indicated for each mode.

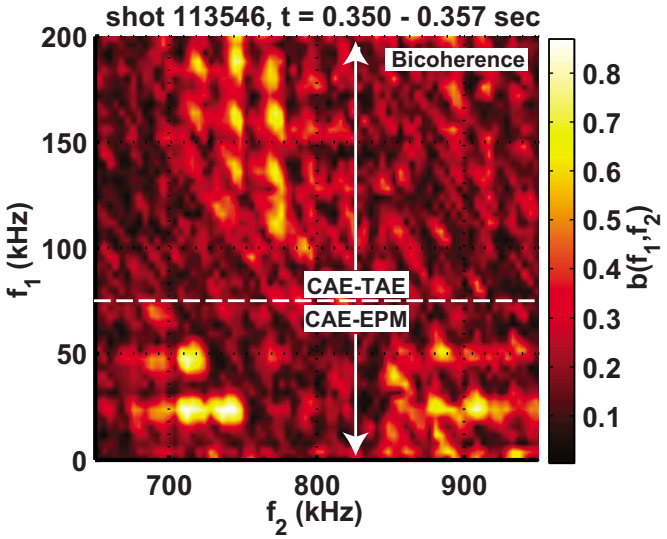

FIG. 4. (Color online) Bicoherence of edge magnetic fluctuation due to CAEs with that due to EPMs and TAEs. Maximum uncertainty is ~0.1.

chirping of their frequencies. The TAEs are identified as such by their characteristic moderate mode numbers and frequencies, which are in the range expected for TAEs under these conditions.

The third group of modes, illustrated in Fig. 2(a), is determined to have toroidal mode numbers of $n\sim-3--12$. Figure 3 shows the magnetic spectrum in this frequency range for an individual burst with toroidal mode numbers indicated. The spectrum is calculated using a 0.5 ms Hanning conditioned record starting at $t=0.357$ s. Modes with frequencies and toroidal mode numbers in this range under these conditions in NSTX have previously been identified as CAEs.[14,5,7] An important aspect of this identification is that the modes have frequencies comparable to but below the fast-ion cyclotron frequency (3.5 MHz at the magnetic axis for these conditions) and that they propagate counter to the beams in the toroidal direction, enabling a Doppler-shifted cyclotron resonance with a significant population of fast ions, which is the source of their drive. Another important aspect of this identification is, as discussed in Ref. 7, the "polarization" (i.e., the direction in the poloidal-toroidal plane) of the magnetic perturbations caused at the plasma edge by the modes shown in Fig. 2(a). These perturbations (not shown) are predominantly parallel to the equilibrium magnetic field, as expected for compressional Alfvén waves.

IV. ANALYSIS

In addition to the three-wave interaction between TAEs and EPMs reported in Ref. 4, three-wave interactions occur independently between the CAEs and both the TAEs and EPMs. As can be seen in Fig. 3, the peaks or modes in the CAE magnetic spectrum can be divided into two groups. The first group has mode numbers $n=-12--7$ and frequencies $f\sim690-810$ kHz. The second has mode numbers $n=-6--3$ and frequencies $f\sim850-925$ kHz. The frequency separation between neighboring modes within each group is ~25 kHz. However the frequency separation between the $n=-7$ and $n=-6$ is a little less than 40 kHz. The frequency separation between neighboring modes within each group implies that pairs of neighboring modes, in combination with the $n=1$, $f\sim25$ kHz EPM, form triplets that satisfy the three-wave matching conditions for frequency and toroidal mode number, $n+n'=n''$ and $f+f'=f''$. Inspection of Fig. 3 also shows that for each mode in the second group with mode number n and frequency f, there is a mode in the first group with mode number $n-5$ that has a frequency $\sim(f-135$ kHz). For instance, the $n=-9$ mode at $f\sim765$ kHz is separated from the $n=-4$ mode at $f\sim900$ kHz by $\Delta n=5$ and $\Delta f=135$ kHz. These pairs of modes, in combination with the dominant $n=5$, $f=135$ kHz TAE that was identified in Ref. 4, also form triplets that satisfy the three-wave matching conditions for frequency and toroidal mode number.

The occurrence of three-wave interaction among these mode triplets is confirmed by calculating the bicoherence of the CAEs with both the EPMs and the TAEs for the time period $t=0.350-0.375$ s using the technique described in Ref. 4. The result of this calculation is shown in Fig. 4. The calculation is performed for magnetic fluctuations obtained by numerically integrating the measurement of an edge Mirnov coil. The integrated coil measurement is divided into records of 0.25 ms long, overlapping by 0.125 ms. The records are conditioned with a Hanning window. It is apparent that the bicoherence is high for both kinds of mode triplets. (Note that some of the peaks in Fig. 4 do not fall at exactly the frequencies of the modes apparent in Fig. 3. This is because Fig. 3 shows the spectrum for a single burst of fluctuations at $t=0.357$ s, while the bicoherence in Fig. 4 is averaged over $t=0.350-0.375$ s, which includes many such bursts. The mode frequencies are somewhat different in each burst. However, the average spectrum (not shown) contains well-defined peaks in the CAE frequency range, although they are much broader than those in individual bursts. All the prominent peaks in the bicoherence (i.e., those with bicoher-

ence $>\sim 0.4$) occur at frequencies corresponding to peaks in the average spectrum. The peaks in the average spectrum are due to the CAEs observed in the bursts, which indicates that the high bicoherence is due to the interactions of those CAEs. Not surprisingly, peaks corresponding to other triplets can also be seen in Fig. 4. TAEs other than the $n=5$, as well as harmonics of the $n=1$ EPM, also participate in the three-wave interactions.

Analysis of the CAEs reveals a significant physical effect of the CAE-EPM interaction. Following the methods described in Ref. 4, the CAE-EPM interaction can be shown to spatially concentrate the CAE fluctuation energy into a toroidally localized wave packet just as the TAE-EPM interaction was shown to do to the TAE fluctuation energy in Ref. 4. Furthermore, this wave packet can be shown to propagate toroidally, remaining locked to a particular phase of the predominantly $n=1$ EPM superposition that was identified in Ref. 4, just as the TAE wave packet was shown to do. As discussed above, the neighboring modes within each group of CAEs have a spacing of $\Delta n=1$ and $\Delta f\sim 25$ kHz. (The significance of the division of the CAEs into two groups is addressed below.) This uniform spacing indicates that the superposition of CAEs has a well-defined toroidal angular group velocity, determined by the spacing, of $2\pi\Delta f/\Delta n \sim 157$ rad/s. Thus, the superposition of CAEs forms a wave packet comprised of a carrier wave and an envelope, where the envelope propagates toroidally at the group velocity. This is the same analysis as was used in Ref. 4 to show that the superposition of TAEs forms a wave packet. The strong bicoherence of pairs of neighboring CAEs with the $n=1$ EPM indicates that the group velocity very precisely matches the toroidal angular phase velocity of the $n=1$ EPM. Consequently, the wave-packet envelope remains locked to a particular phase of the EPM superposition as it propagates toroidally, just as the TAE wave-packet envelope was shown to do.

The CAE and TAE wave packets and the phase locking of their envelopes to the EPM are illustrated in Fig. 5. Figure 5 shows the magnetic fluctuations due to the three types of modes measured by three Mirnov coils near the plasma edge at toroidal angles of 30°, 180°, and 330°. The coil measurements, which are numerically integrated to give the poloidal magnetic field fluctuation, are bandpass filtered, just as in the analysis in Ref. 4, in order to isolate the total contributions for each type of mode. (The TAE and CAE fluctuations shown in Fig. 5 are multiplied by factors of 5.5 and 120, respectively, so that they can be resolved on the scale of EPM.) The peak amplitude of the EPM, TAE, and CAE fluctuations shown in Fig. 5 are ~2, ~0.4, and ~0.01 G, respectively. As is evident in the figure, each coil successively observes both the CAE and TAE wave packets as they propagate around the torus. The phase locking of both wave-packet envelopes to the EPM is also apparent. Diagonal lines—drawn through the rising edge of the EPM as observed by each coil—guide the eyes, making this clear. This spatial redistribution of the CAE and TAE fluctuation energy is important because it will modify the effect the modes have on fast-ion orbits. Consequently, it will modify their effects

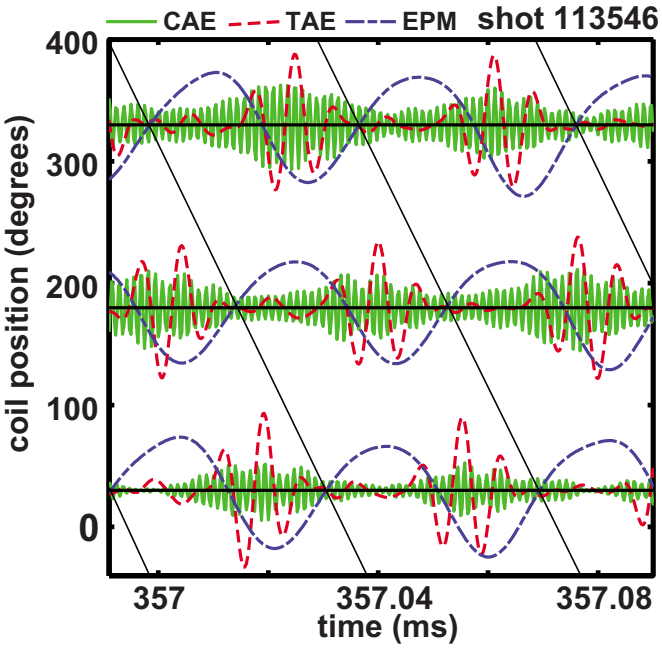

FIG. 5. (Color online) Separate contributions of the EPMs, TAEs, and CAEs to the edge magnetic fluctuations at three separate toroidal locations at 30°, 180°, and 330°. (TAEs and CAEs normalized for comparison with EPMs.) Diagonal lines are drawn through the rising edge of the EPM oscillation as guides.

on fast-ion transport and the role they play in the observed fast-ion loss.

Further analysis of the CAEs reveals a significant physical effect of the CAE-TAE interaction. It shows that CAE-TAE interaction modulates the fluctuation power in the CAE band. Recall that the spectrum of CAEs can be divided into two groups where each mode in the higher frequency group has a spacing of $\Delta n=5$ and $\Delta f\sim 135$ kHz with a mode in the lower frequency group. Each group by itself satisfies the conditions described above for its superposition to form a wave packet phase locked to the $n=1$ EPM. However, the spacing between the two superpositions, $\Delta n=5$ and $\Delta f \sim 135$ kHz, indicates that their carrier waves have effective n and f that differ by $\Delta n=5$ and $\Delta f\sim 135$ kHz. Consequently, the two carrier waves beat against each other. The strong bicoherence of the CAEs with the dominant $n=5$, $f\sim 135$ kHz TAE indicates that the toroidal angular velocity of this beat wave, $2\pi\Delta f/\Delta n\sim 170$ rad/s, matches very precisely the toroidal angular phase velocity of the dominant TAE. Thus, the beat wave, which can be viewed as a modulation of the total CAE wave-packet amplitude, strongly correlates in time and toroidal location with the dominant TAE. The strong bicoherence of the CAEs with other TAEs shows that they participate in the amplitude modulation as well, indicating that the fluctuation power in the CAE band is modulated by not just the dominant TAE but by the full TAE wave packet. Further analysis discussed below confirms this.

The modulation of the fluctuation power in the CAE band by the TAEs is illustrated in Fig. 6. Figure 6 shows the TAE magnetic fluctuation at three toroidal locations (also illustrated in Fig. 5). For comparison, the *time-dependent power* in the CAE band is calculated by squaring the CAE

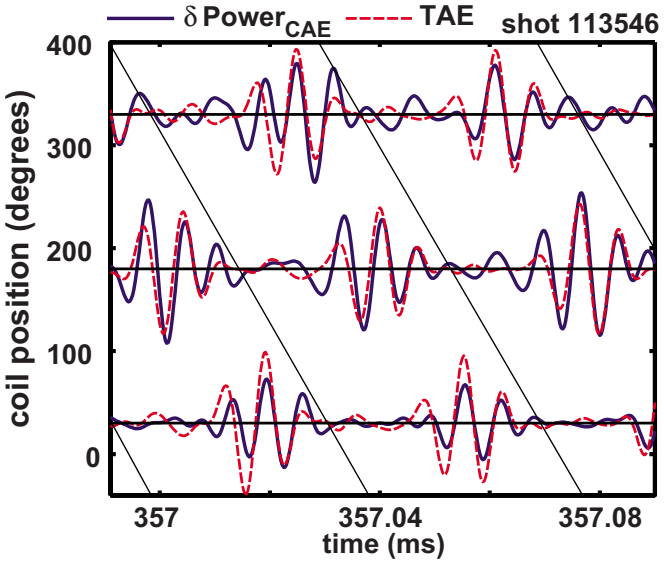

FIG. 6. (Color online) TAE edge magnetic fluctuation. Also, time-dependent power in CAE magnetic fluctuation filtered to isolated modulations in frequency band corresponding to TAEs. Diagonal lines corresponding to the rising edge of the EPM oscillation are shown as guides.

magnetic fluctuation (shown in Fig. 5) and averaging over the CAE oscillation time scale. The result, bandpass filtered to keep only the frequencies in the TAE band, is also shown in Fig. 6. The observed amplitude modulation amounts to ~10% of the peak fluctuation power in the CAE wave packet over the time period shown. In the figure, both curves are rescaled by arbitrary factors to facilitate direct comparison. It is apparent from the figure that the modulation of the CAE power is highly correlated with the TAE oscillation. Comparison of the measurements for the three coils shown in Fig. 6 confirms that the correlation is not just temporal but spatial as well. The strongest modulation of the CAE power is spatially localized to the region of the TAE wave packet. Notably, it is also correlated with the oscillation of the carrier wave of the TAE wave packet. These observations confirm that interaction with the TAE wave packet modulates the CAE wave packet that is formed by interaction with the EPMs, partially subdividing it into smaller wave packets whose envelopes are phase locked to the carrier wave of the TAE wave packet. (The subdivision is partial in the sense that the modulation is not 100%.)

V. DISCUSSION

The observed spatial redistribution of the CAE fluctuation power will have a significant impact on fast-ion transport. An obvious consequence of the concentration of fluctuation power is that the magnetic perturbation in the region of the CAE wave packet is amplified over what the same fluctuation energy would be likely to produce if the individual CAEs had random phases. The more concentrated the energy becomes, the greater the amplification will be. The same is true, of course, for TAEs. The amplified magnetic perturbation will produce a larger perturbation to resonant fast-ion orbits, which will enhance the resulting fast-ion transport, and possibly the fast-ion loss as well. The effect of the redistribution is, of course, complicated by the inherently toroidally localized structure of the wave packet. The amplification of the magnetic perturbation in the region of the wave packet comes at the cost of a reduced magnetic perturbation elsewhere. This will lead to a reduction in the fast-ion transport there, and possibly of the losses as well. However, since the effect of magnetic perturbations on fast-ion orbits is strongly nonlinear, the reductions in transport and loss away from the wave packet will not necessarily balance the increase inside the wave packet. Given these complications, assessing the effect of the observed redistribution of fluctuation energy on fast-ion transport will require the use of powerful computational tools such as a code to calculate perturbed fast-ion orbits.

VI. SUMMARY

In summary, simultaneous three-wave interactions of CAEs with both EPMs and TAEs are conclusively identified in NSTX beam-heated plasmas. Triplets of modes are identified satisfying the three-wave matching conditions for frequency and toroidal mode number. Three-wave interaction is confirmed for these triplets by high levels of bicoherence. The nonlinear interaction of the CAEs with EPMs is shown to spatially concentrate the fluctuation energy of the CAEs into a toroidally localized wave packet, just the TAE-EPM interaction was shown to do to the TAE energy in Ref. 4. The envelope of the CAE wave packet is shown to propagate phase locked to the EPM superposition just as that of the TAE wave packet was shown to do in Ref. 4. The nonlinear interaction of CAEs with TAEs is shown to subdivide the CAE wave packet into smaller wave packets whose envelopes propagate phase locked to the carrier wave of the TAE wave packet.

The observed spatial redistribution of CAE and TAE fluctuation energies is important because the magnetic perturbation in the region of a wave packet is amplified over what the same energy would be likely to produce if the phases of the individual modes were random. This amplification will enhance the perturbation of the resonant fast-ion orbits and the resulting fast-ion transport, and possibly the fast-ion loss as well. However, the overall effect of the redistribution will be complicated because the magnetic perturbation is reduced away from the wave packet. Fast-ion transport, and possibly fast-ion loss, will be reduced there, although this may not balance the increases in the region of the wave packet.

ACKNOWLEDGMENTS

The authors wish to thank T. Carter, B. Brugman, and T. Rhodes of the University of California, Los Angeles, as well as W. W. Heidbrink of the University of California, Irvine, for useful discussions, and E. Ruskov, also of the University of California, Irvine, for assistance with TRANSP modeling. This work was supported by U.S. DOE Grant Nos. DE-FG02-99ER54527 and DE-AC02-76CH03073.

[1]A. Fasoli, C. Gormenzano, H. L. Berk, B. Breizman, S. Briguglio, D. S. Darrow, N. Gorelenkov, W. W. Heidbrink, A. Jaun, S. V. Konovalov, R. Nazikian, J.-M. Noterdaeme, S. Sharapov, K. Shinohara, D. Testa, K. Tobita, Y. Todo, G. Vlad, and F. Zonca, Nucl. Fusion **47**, S264 (2007).
[2]M. Ono, S. M. Kaye, Y.-K. M. Peng, G. Barnes, W. Blanchard, M. D. Carter, J. Chrzanowski, L. Dudek, R. Ewig, D. Gates, R. E. Hatcher, T. Jarboe, S. C. Jardin, D. Johnson, R. Kaita, M. Kalish, C. E. Kessel, H. W. Kugel, R. Maingi, R. Majeski, J. Manickam, B. McCormack, J. Menard, D. Mueller, B. A. Nelson, B. E. Nelson, C. Neumeyer, G. Oliaro, F. Paoletti, R. Parsells, E. Perry, N. Pomphrey, S. Ramakrishnan, R. Raman, G. Rewoldt, J. Robinson, A. L. Roquemore, P. Ryan, S. Sabbagh, D. Swain, E. J. Synakowski, M. Viola, M. Williams, J. R. Wilson, and NSTX Team, Nucl. Fusion **40**, 557 (2000).
[3]Y. C. Kim and E. J. Powers, Phys. Fluids **21**, 1452 (1978).
[4]N. A. Crocker, W. A. Peebles, S. Kubota, E. D. Fredrickson, S. M. Kaye, B. P. LeBlanc, and J. E. Menard, Phys. Rev. Lett. **97**, 045002 (2006).
[5]E. D. Fredrickson, C. Z. Cheng, L. Chen, D. Darrow, N. N. Gorelenkov, D. Johnson, S. Kaye, S. Kubota, J. Menard, and R. B. White, Europhys. Conf. Abstr. **26B**, 1.104 (2002).
[6]E. D. Fredrickson, C. Z. Cheng, D. Darrow, G. Fu, N. N. Gorelenkov, G. Kramer, S. S. Medley, J. Menard, L. Roquemore, D. Stutman, and R. B. White, Phys. Plasmas **10**, 2852 (2003).
[7]E. D. Fredrickson, R. E. Bell, D. S. Darrow, G. Y. Fu, N. N. Gorelenkov, B. P. LeBlanc, S. S. Medley, J. E. Menard, H. Park, A. L. Roquemore, W. W. Heidbrink, S. A. Sabbagh, D. Stutman, K. Tritz, N. A. Crocker, S. Kubota, W. Peebles, K. C. Lee, and F. M. Levinton, Phys. Plasmas **13**, 056109 (2006).
[8]K. McGuire, R. Goldston, M. Bell, M. Bitter, K. Bol, K. Brau, D. Buchenauer, T. Crowley, S. Davis, F. Dylla, H. Eubank, H. Fishman, R. Fonck, B. Grek, R. Grimm, R. Hawryluk, H. Hsuan, R. Hulse, R. Izzo, R. Kaita, S. Kaye, H. Kugel, D. Johnson, J. Manickam, D. Manos, D. Mansfield, E. Mazzucato, R. McCann, D. McCune, D. Monticello, R. Motley, D. Mueller, K. Oasa, M. Okabayashi, K. Owens, W. Park, M. Reusch, N. Sauthoff, G. Schmidt, S. Sesnic, J. Strachan, C. Surko, R. Slusher, H. Takahashi, F. Tenney, P. Thomas, H. Towner, J. Valley, and R. White, Phys. Rev. Lett. **50**, 891 (1983).
[9]R. B. White, R. J. Goldston, K. McGuire, A. H. Boozer, D. A. Monticello, and W. Park, Phys. Fluids **26**, 2958 (1983).
[10]L. Chen, R. B. White, and M. N. Rosenbluth, Phys. Rev. Lett. **52**, 1122 (1984).
[11]E. Fredrickson, L. Chen, and R. White, Nucl. Fusion **43**, 1258 (2003).
[12]C. Z. Cheng, L. Chen, and M. S. Chance, Ann. Phys. (N.Y.) **161**, 21 (1985).
[13]C. Z. Cheng and M. S. Chance, Phys. Fluids **29**, 3695 (1986).
[14]E. D. Fredrickson, N. Gorelenkov, C. Z. Cheng, R. Bell, D. Darrow, D. Johnson, S. Kaye, B. LeBlanc, J. Menard, S. Kubota, and W. Peebles, Phys. Rev. Lett. **87**, 145001 (2001).
[15]S. M. Mahajan and D. W. Ross, Phys. Fluids **26**, 2561 (1983).
[16]B. Coppi, S. Cowley, R. Kulsrud, P. Detragiache, and F. Pegoraro, Phys. Fluids **29**, 4060 (1986).
[17]N. N. Gorelenkov and C. Z. Cheng, Nucl. Fusion **35**, 1743 (1995).
[18]J. Hosea, R. E. Bell, B. P. LeBlanc, C. K. Phillips, G. Taylor, E. Valeo, J. R. Wilson, E. F. Jaeger, P. M. Ryan, J. Wilgen, H. Yuh, F. Levinton, S. Sabbagh, K. Tritz, J. Parker, P. T. Bonoli, R. Harvey, and NSTX Team, Phys. Plasmas **15**, 056104 (2008).
[19]B. P. LeBlanc, R. E. Bell, D. W. Johnson, D. E. Hoffman, D. C. Long, and R. W. Palladino, Rev. Sci. Instrum. **74**, 1659 (2003).
[20]K. L. Wong, R. J. Fonck, S. F. Paul, D. R. Roberts, E. D. Fredrickson, R. Nazikian, H. K. Park, M. Bell, N. L. Bretz, R. Budny, S. Cohen, G. W. Hammett, F. C. Jobes, D. M. Meade, S. S. Medley, D. Mueller, Y. Nagayama, D. K. Owens, and E. J. Synakowski, Phys. Rev. Lett. **66**, 1874 (1991).
[21]W. W. Heidbrink, E. J. Strait, E. Doyle, G. Sager, and R. T. Snider, Nucl. Fusion **31**, 1635 (1991).
[22]S. A. Sabbagh, S. M. Kaye, J. Menard, F. Paoletti, M. Bell, R. E. Bell, J. M. Bialek, M. Bitter, E. D. Fredrickson, D. A. Gates, A. H. Glasser, H. Kugel, L. L. Lao, B. P. LeBlanc, R. Maingi, R. J. Maqueda, E. Mazzucato, D. Mueller, M. Ono, S. F. Paul, M. Peng, C. H. Skinner, D. Stutman, G. A. Wurden, W. Zhu, and NSTX Research Team, Nucl. Fusion **41**, 1601 (2001).
[23]L. L. Lao, H. St. John, R. D. Stambaugh, A. G. Kellman, and W. Pfeiffer, Nucl. Fusion **25**, 1611 (1985).
[24]J. P. H. E. Ongena, M. Evrard, and D. McCune, Fusion Sci. Technol. **53**, 367 (2008).
[25]R. V. Budny, Nucl. Fusion **34**, 1247 (1994).
[26]D. Johnson and NSTX Team, Plasma Phys. Controlled Fusion **45**, 1975 (2003).
[27]R. E. Bell, B. P. LeBlanc, C. Bourdelle, D. R. Ernst, E. D. Fredrickson, D. A. Gates, J. C. Hosea, D. W. Johnson, S. M. Kaye, R. Maingi, S. Medley, J. E. Menard, D. Mueller, M. Ono, F. Paoletti, M. Peng, S. A. Sabbagh, D. Stutman, D. W. Swaina, E. J. Synakowski, and J. R. Wilson, Europhys. Conf. Abstr. **25A**, 1021 (2001).